

RESEARCH ARTICLE

A family of ROP proteins that suppresses actin dynamics, and is essential for polarized growth and cell adhesion

Graham M. Burkart^{1,2,*}, Tobias I. Baskin¹ and Magdalena Bezanilla^{1,‡}

ABSTRACT

In plants, the ROP family of small GTPases has been implicated in the polarized growth of tip-growing cells, such as root hairs and pollen tubes; however, most of the data derive from overexpressing ROP genes or constitutively active and dominant-negative isoforms, whereas confirmation by using loss-of-function studies has generally been lacking. Here, in the model moss *Physcomitrella patens*, we study ROP signaling during tip growth by using a loss-of-function approach based on RNA interference (RNAi) to silence the entire moss ROP family. We find that plants with reduced expression of ROP genes, in addition to failing to initiate tip growth, have perturbed cell wall staining, reduced cell adhesion and have increased actin-filament dynamics. Although plants subjected to RNAi against the ROP family also have reduced microtubule dynamics, this reduction is not specific to loss of ROP genes, as it occurs when actin function is compromised chemically or genetically. Our data suggest that ROP proteins polarize the actin cytoskeleton by suppressing actin-filament dynamics, leading to an increase in actin filaments at the site of polarized secretion.

KEY WORDS: GTPase, Actin, Polarity

INTRODUCTION

In eukaryotes, the small Rho-like GTPases are central regulators of cell division, polarity and morphogenesis. Fungi and animals have three distinct families (Rho, Cdc42 and RAC), whereas plants have a single family, known as Rho of plants (ROP; sometimes called RAC because of their greater resemblance to that clade). In the GDP-bound state, ROP proteins are cytosolic and inactive; in the GTP-bound state, they are active and associate with membranes, where they have been implicated in moderating numerous cellular processes, including cell morphogenesis, polarized growth, and responses to hormone and oxygen levels (Craddock et al., 2012).

The early evolution of the ROP family remains enigmatic as ROP genes have not been identified in some green algae, such as *Chlamydomonas reinhardtii* and *Chlorella variabilis*, but one ROP gene is present in the green alga *Ostreococcus spp* (Fowler, 2010). Basal land plants have relatively few ROP genes. For example, the moss *Physcomitrella patens* has four and the lycophyte *Selaginella molendorffii* has two. All ROP sequences in algae and non-seed plants terminate with a prenylation motif (the CaaX box) and are known as type I. The ROP gene family expanded in seed plants, first

by introducing a second family, type II, in which prenylation was lost, and these are thought to have evolved from type I through insertion of an additional 3' intron (Winge et al., 2000). In angiosperms, further expansion has culminated in relatively large ROP gene families. For example, *Arabidopsis thaliana* has 11 ROP-family members, eight in class I and three in class II.

In angiosperms, the amplification and diversification of ROP proteins has been explored through efforts to link distinct family members to distinct cellular processes (Craddock et al., 2012). ROP proteins have been implicated in the polarized expansion of root hairs [in *Arabidopsis thaliana* (*AtROP2* and *AtROP4*; also known as *ARAC4* and *ARAC5*, respectively)] and pollen tubes (*AtROPI*, *AtROP3* and *AtROP5*; also known as *ARAC11*, *ARAC1* and *ARAC6*, respectively) (Gu et al., 2006; Li et al., 1999; Jones et al., 2002; Fu et al., 2002, 2001). In the latter cell type, *AtROPI* has been linked to the modulation of Ca²⁺ influx at the cell tip (Li et al., 1999; Gu et al., 2005). In cell shape and tissue patterning, such as in the formation of leaf epidermal pavement cells, ROP-family members have been alleged to coordinate the antagonistic interaction of actin and microtubule cytoskeletons (*AtROP2*, *AtROP4* and *AtROP6*) (Craddock et al., 2012; Lin et al., 2015). ROP proteins have also been implicated in xylem differentiation (Brembu et al., 2005; Foucart et al., 2009). *AtROPI1*, through its effector *MIDD1*, induces the disassembly of cortical microtubules during the formation of secondary cell walls in xylem cells (Oda and Fukuda, 2012).

Many studies on the function of ROP proteins in plants have relied on expressing native or aberrant versions (e.g. constitutively active and dominant-negative isoforms) at high levels. Although popular, such approaches are problematic (Gibson et al., 2013). One way to grasp this is by recalling that many genes are regulated by dosage and thus alter the phenotype when their expression level is merely doubled (Veitia and Birchler, 2010). In general, signaling pathways, being cooperative and webbed, are sensitive to stoichiometry. To elucidate a mechanism, rather than merely infer an influence, it is invaluable to keep expression levels native and, in addition, to characterize the consequences of loss of function.

Unfortunately, for inferences about ROP activity in plants, confirmation from loss-of-function studies has been scarce. A notable exception comes from micro-injection studies, where antibodies against *AtROPI* inhibit pollen tube growth (Lin and Yang, 1997). Consistently, targeting ROP genes with antisense oligonucleotides disturbs pollen tube growth, with varying degrees of severity. Some pollen tubes are significantly wider, and others no longer grow straight (Camacho and Malhó, 2003; Mizuta and Higashiyama, 2014). However, in general, ROP-knockout plants have surprisingly mild defects in cell polarity and polarized growth. In *A. thaliana*, a *rop6* T-DNA insertion line increases lateral root density, but apparently does not impair root hair growth (Lin et al., 2012). In fact, in *rop1/rop6* double-mutant plants, the frequency of root hair branching is increased, but root hairs are still polarized and grow to similar lengths as in the wild type (Venus and Oelmüller,

¹Department of Biology, University of Massachusetts-Amherst, 611 N. Pleasant Street, Amherst, MA 01003, USA. ²Plant Biology Graduate Program, University of Massachusetts-Amherst, 611 N. Pleasant Street, Amherst, MA 01003, USA. *Present address: Department of Biology, Washington University in St. Louis, 1 Brookings Drive, St. Louis, MO 63130, USA.

[‡]Author for correspondence (bezanilla@bio.umass.edu)

2013). When ROP loss-of-function was engineered previously, by expressing a bacterial toxin transgene in *A. thaliana* that is known to inhibit ROP4 *in vitro*, plants formed few, if any, root hairs (Singh et al., 2013). Although this is a severe phenotype, the specificity of the effects of the transgene *in vivo* requires confirmation. The lack of severe tip-growth defects observed in ROP-knockout mutants is plausibly explained by redundancy; nevertheless, the specific actions performed by ROP proteins to polarize plant cells remain obscure.

With only four ROP genes and the amenable reverse genetics in *P. patens*, moss provides an excellent system to analyze ROP function in cell polarity and morphogenesis using a loss-of-function approach. In doing so, it might also be possible to infer the ancestral function of the ROP GTPase in land plants. Here, using a combination of genetics and live-cell imaging, we show that the moss ROP proteins are functionally redundant and essential for polarized growth. Additionally, they appear to condition the assembly of the cell wall and to negatively regulate the dynamics of actin filaments.

RESULTS

Deletion of a single ROP locus reduces the expression of the remaining ROP genes

The four ROP genes in *P. patens* are strikingly similar (Eklund et al., 2010). In fact, the amino acid sequences encoded are identical in ROP1 and ROP4, differ by one amino acid between ROP1 and ROP4 and between ROP2 and ROP3, and differ by two amino acids between ROP2 and ROP3. We reasoned that, with such high sequence similarity, these genes are functionally redundant. To investigate this possibility, we analyzed the expression of each ROP gene in wild-type protonemal tissue by using quantitative real-time reverse transcriptase PCR (qRT-PCR). Interestingly, ROP3 and ROP4 transcripts comprised the vast majority (~90%) of the total ROP gene transcript pool (Fig. 1A). However, because the ROP genes have a high sequence similarity at the nucleotide level, it is

possible that ROP3 and ROP4 transcripts are over represented owing to mis-amplification. To ensure that the qRT-PCR primers were specific for each ROP gene, we generated stable lines containing single-gene knockouts of each ROP using homologous recombination to replace the locus with a hygromycin-resistance marker and then analyzed expression of the ROP genes. In all four single-knockout lines, we failed to amplify the transcript from the deleted ROP gene (Fig. 1B), demonstrating that the qRT-PCR primers were specific and confirming that ROP3 and ROP4 were the most highly expressed ROP genes.

Surprisingly, knocking out a single ROP gene (supplementary material Fig. S1) negatively impacted the expression of the remaining ROP genes (Fig. 1B). In particular, deletion of ROP2, which only contributed to ~1% of the total ROP transcript pool, resulted in a 50–60% reduction of ROP1, ROP3 and ROP4. Deletion of ROP3 reduced expression of ROP1, ROP2 and ROP4 to a similar extent (Fig. 1B). Although the single-gene knockouts of each ROP gene were viable, they were smaller than wild type (Fig. 1C,D). Interestingly, $\Delta rop2$ and $\Delta rop3$ had the strongest effect on total ROP gene expression and the most significant decreases in plant area (45 and 40%, respectively), whereas $\Delta rop1$ and $\Delta rop4$ impacted the total expression of genes the least and affected growth modestly, reducing plant area by approximately 25% (Fig. 1D).

Because deletion of a single ROP locus negatively affected the expression of ROP genes from the other three loci, we reasoned that interpretation of phenotypic analyses using additional deletion mutants might be complicated by interactions amongst these loci. Thus, as an alternative, we used transient RNA interference (RNAi) to simultaneously silence all four ROP genes without altering the genomic context of each gene.

ROP proteins are essential for tip growth

We used two different constructs to silence ROP genes using RNAi (Fig. 2A). In the first one (*ROP4cds*), the construct contained a

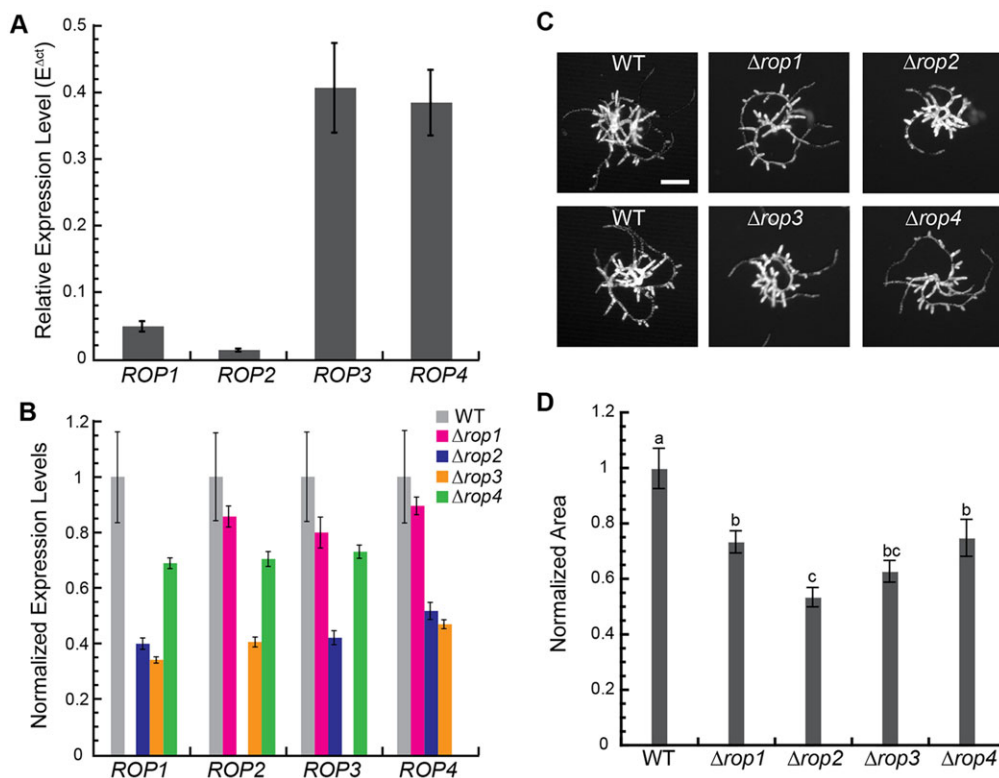


Fig. 1. Expression levels of ROP genes and the growth phenotypes in wild-type and single-ROP-deletion lines. (A) Relative expression of ROP genes in 8-day-old wild-type moss plants regenerated from protoplasts, normalized to that of *UBIQUITIN10*. E is the amplification efficiency. (B) Relative expression levels in 8-day-old plants regenerated from protoplasts of single-ROP-deletion lines, normalized to the expression levels in wild type. All expression levels were first normalized to *UBIQUITIN10*. (C) Micrographs of chlorophyll autofluorescence of 6-day-old ROP-deletion and wild-type plants regenerated from protoplasts. Scale bar: 200 μ m. (D) Quantification of the plant area is based on the area of the chlorophyll autofluorescence and is presented normalized to that of wild-type plants ($n=75$ plants for each line). The letters above the bars indicate statistical groups with $\alpha=0.05$ using ANOVA. Error bars represent s.e.m.

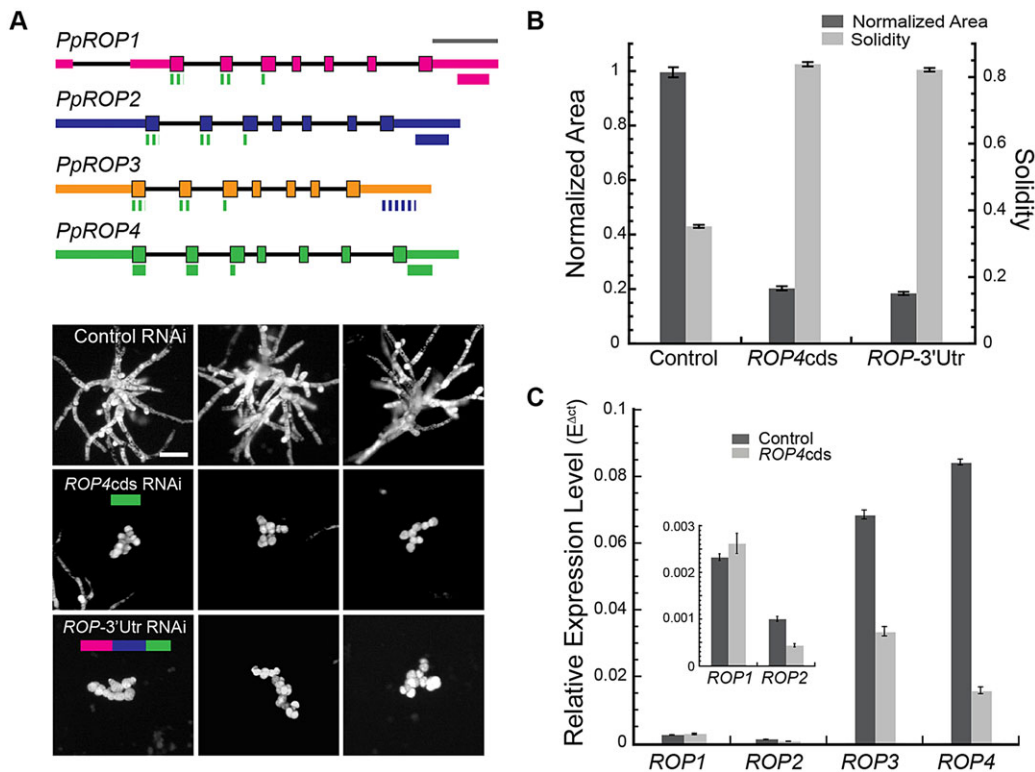


Fig. 2. ROP genes are essential for polarized growth. (A) Gene models of the *Physcomitrella patens* ROP family are shown with exons indicated by boxes and introns by thin black lines. Coding and untranslated regions are denoted by thick and thin boxes, respectively. The lines underneath the gene models represent sequence regions that are targeted by ROP RNAi constructs. Solid lines indicate that the denoted sequence was used in the RNAi construct, whereas dashed lines indicate highly similar sequence regions that are targeted by the RNAi constructs *ROP4cds* and *ROP-3'Utr*. Scale bar is 500 bp. Representative chlorophyll autofluorescence images of 7-day-old NLS4 plants regenerated from protoplasts expressing the indicated RNAi constructs are shown below the gene models. Scale bar: 100 μ m. (B) Quantification of plant area (dark gray) and solidity (light gray) for control RNAi ($n=450$ plants), *ROP4cds* ($n=200$ plants) and *ROP-3'Utr* ($n=490$ plants). The area is based on chlorophyll autofluorescence and is presented having been normalized to that of control plants. Solidity is defined as convex hull area divided by area. (C) Relative expression levels of the ROP genes normalized to that of *UBIQUITIN10* in 8-day-old plants expressing control (dark gray) and *ROP4cds* (light gray) RNAi constructs. E is the amplification efficiency. Inset in C, the relative expression levels of *ROP1* and *ROP2* normalized to that of *UBIQUITIN10*. Error bars represent s.e.m.

single cDNA fragment from *ROP4* that was 89.87–90.75% identical to the sequences of the other three ROP genes. In the second one (*ROP-3'Utr*), the construct contained 190–256 bp from each of the 3' untranslated regions of *ROP1*, *ROP2* and *ROP4*. The equivalent region from *ROP3* was omitted because it was 85% identical to 159 bp of the *ROP2*-targeting sequence. Considering that both of these RNAi constructs had such high sequence identity to the target genes, we expected that both should effectively target all four ROP genes.

We used an optimized transient-RNAi assay that enables rapid identification of plants in which the genes have been silenced (Bezanilla et al., 2005). In this assay, RNAi constructs containing inverted repeats of target-gene sequences fused to β -glucuronidase (GUS) sequences are transformed into a moss line (NLS4) that stably expresses a nuclear-localized green fluorescent protein (GFP) fused to GUS. This permits simultaneous silencing of the target gene and of the GFP–GUS fusion reporter. The control RNAi construct only contains inverted repeats of GUS sequences. One week after transformation, actively silenced plants, identified by lack of nuclear GFP fluorescence, are analyzed.

Control RNAi plants had elongated branching protonemal cells, indistinguishable from un-transformed regenerating moss plants. By contrast, expression of *ROP4cds* or *ROP-3'Utr* yielded plants comprising small spherical cells (Fig. 2A). To quantify the effects of RNAi of ROP genes (ROP RNAi) on plant area and morphology,

we measured plant area and solidity, the latter being a ratio of the total plant area to the convex hull area. A solidity value equal to 1 reflects a body without indentations, and solidity values fall as indentations increase. Silencing with either of the ROP RNAi constructs decreased plant area substantially and increased solidity dramatically (Fig. 2B).

To determine whether the observed phenotype results from a reduction in ROP gene expression, we analyzed the expression of ROP genes in the regenerated plants. Notably, by comparing relative expression levels (Fig. 1A, Fig. 2C), control RNAi plants had only about a fifth as much total ROP gene transcript pools as compared with that of wild-type tissue, although the relative abundance of the four loci remained approximately similar. The reduction in expression might have resulted from different growth conditions because the RNAi plants were grown on selection medium following protoplast regeneration. Be that as it may, in *ROP4cds* RNAi plants, although the effect on *ROP4* was the strongest, the total transcript pool was reduced by 66% (Fig. 2C). In view of the reduction in expression that occurred during protoplast regeneration, this amounts to a large absolute reduction in expression of the ROP genes. Because plants that had been subjected to RNAi had to be transferred one at a time by hand to RNA extraction buffer, this analysis was not repeated for *ROP-3'Utr* RNAi, and all subsequent phenotypic analyses were performed using the *ROP4cds* RNAi construct. Nevertheless, these data demonstrate that unpolarized

*ROP4*cds RNAi plants had a significantly reduced level of ROP transcripts, indicating that ROP genes are essential for tip growth.

ROP RNAi plants have a cell adhesion defect

In performing the above RNA quantification, we noticed that when transferred with a fine metal needle, *ROP* RNAi plants fell apart easily. To investigate this, we picked 8-day-old plants into a water droplet and sonicated them. Because *ROP* RNAi plants comprised small spherical cells, we used plants in which two redundant *MyoXI* genes (*MYOXIA*, SwissProt ID D6R266; *MYOXIB*, SwissProt ID D6R267) had been silenced (*MyoXI* RNAi) as controls for cell shape, because the size and shape of the *MyoXI* RNAi plants are indistinguishable from that of the *ROP* RNAi plants (Vidali et al., 2010). Interestingly, controls and *MyoXI* RNAi plants remained mostly intact, the *ROP* RNAi plants readily broke apart into small clumps or individual cells (Fig. 3A,B). Evidently, the loss of ROP activity reduced cell adhesion.

Because pectin is known to underlie cell adhesion (Lord and Mollet, 2002), we investigated pectin content in the cell wall by staining for pectin, trying dyes including Ruthenium Red, Toluidine Blue and propidium iodide. However, the dyes stained wild-type plants inconsistently, limiting their usefulness. As an alternative, we manipulated Ca^{2+} in the cell wall. Typically, removing Ca^{2+} from the cell wall destabilizes pectin, resulting in weaker adhesion, whereas adding Ca^{2+} has the converse effect (Hepler, 2005). We expected that with lowered Ca^{2+} , mild sonication would separate cells in control and *MyoXI* RNAi plants, and in contrast, with increased Ca^{2+} , sonication would become less effective in separating cells in the *ROP* RNAi plants. However, when plants were incubated in excess 100 mM Ca^{2+} or in 250 mM EGTCA (to remove the Ca^{2+} from the cell wall), adhesion in neither controls nor RNAi plants was appreciably altered (data not shown), suggesting that cell adhesion in moss depends negligibly on Ca^{2+} cross-bridges in pectin.

Next, we investigated cellulose and callose because both are major components of the moss cell wall (Roberts et al., 2012). We isolated and stained plants with the following dyes – Calcofluor White (stains predominantly cellulose), Aniline Blue (stains callose) and Fast Scarlet 4B (stains cellulose) (Fig. 4A). Interestingly, the *ROP* RNAi plants had a modest decrease in staining with Aniline Blue and a roughly 50% decrease in staining with both Calcofluor and Fast Scarlet (Fig. 4A,B). It is evident that this was not simply an effect of cell geometry by comparing with the staining of *MyoXI* RNAi plants,

which was largely comparable to that of controls. These data point to lowered amounts of callose and cellulose in the cell wall of *ROP* RNAi plants, which could relate to the lower level of cell adhesion.

However, because staining of the cell wall also depends on access of the dye to its target, we used polarized-light microscopy to detect cellulose, taking advantage of its birefringence (Fig. 4A). Our microscope used circularly polarized light and was thus insensitive to the orientation of the sample on the stage (see Materials and Methods); we quantified retardance at either side of the cell, where light passes ‘end-on’ through the cell wall. In contrast to the dye results, cell wall retardance increased in *ROP* RNAi plants and decreased in *MyoXI* RNAi plants (Fig. 4C). Based on cell geometry alone, we expected an increase in retardance in both *ROP* RNAi and *MyoXI* RNAi cells because their diameter was increased and, therefore, light at the sides of the cell passes through more of the cell wall. Therefore, decreased retardance for *MyoXI* RNAi is compelling evidence that this protein plays a positive role in cellulose synthesis, possibly through promoting transport or secretion of vesicles that contain cellulose synthase. By contrast, the increased retardance for *ROP* RNAi plants can be explained by cell size. Consequently, the decrease in the signal from Calcofluor and Fast Scarlet indicates that the dyes had restricted access to cellulose and, thus, that the cell wall structure was altered. Taken together, reductions in both cell wall staining and cell adhesion indicate a role for ROP proteins in the assembly of the cell wall.

A ROP-RNAi-insensitive line exhibits tip growth

To test whether a single ROP gene can rescue *ROP* RNAi phenotypes, we performed a transient complementation assay whereby we co-transformed the *ROP-3'Utr* RNAi construct with a ROP expression construct that lacked the 3'-untranslated region. In these expression constructs, the maize ubiquitin promoter drove expression of either *ROP3* or *ROP4* (UBI-*ROP3* and UBI-*ROP4*, respectively). In contrast to transformation with *ROP-3'Utr* alone, which yielded hundreds of mutant plants per transformation, we were unable to recover plants in which ROP genes were silenced and the UBI-*ROP3* or UBI-*ROP4* expression constructs were also expressed. In fact, transformation of UBI-*ROP3* or UBI-*ROP4* alone resulted in no transformants, suggesting that overexpression of ROP proteins is incompatible with regeneration, possibly because of lethality. Transformants were also lacking when the expression constructs used putative ROP promoters (~2-kb sequence upstream

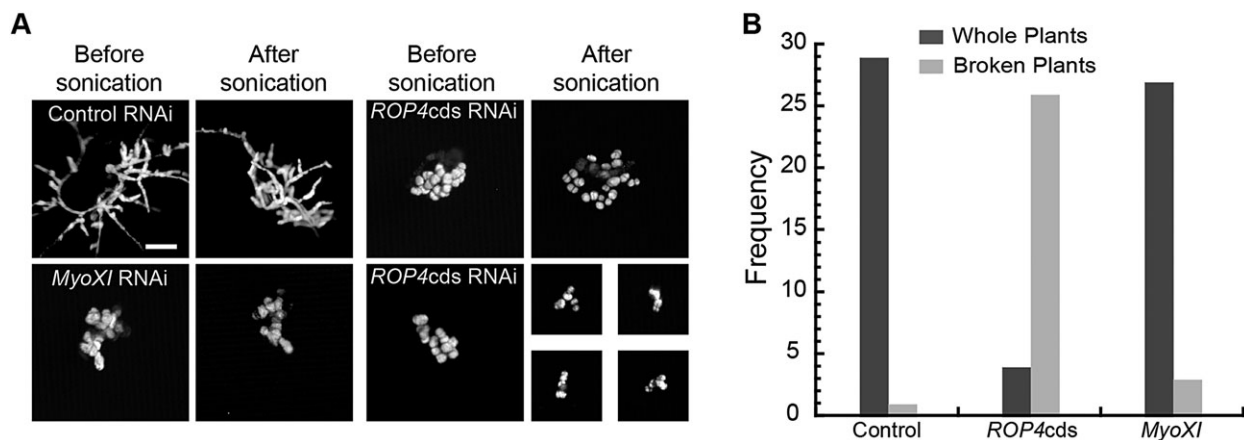


Fig. 3. ROP RNAi plants have a cell adhesion defect. (A) Micrographs of chlorophyll autofluorescence of 8-day-old NLS4 plants expressing control, *ROP4cds* or *MyoXI* RNAi constructs before and after mild sonication. Scale bar: 100 μm . (B) Frequency of whole (dark gray) and broken (light gray) plants after mild sonication of 30 8-day-old NLS4 plants expressing control, *ROP4cds* or *MyoXI* RNAi constructs.

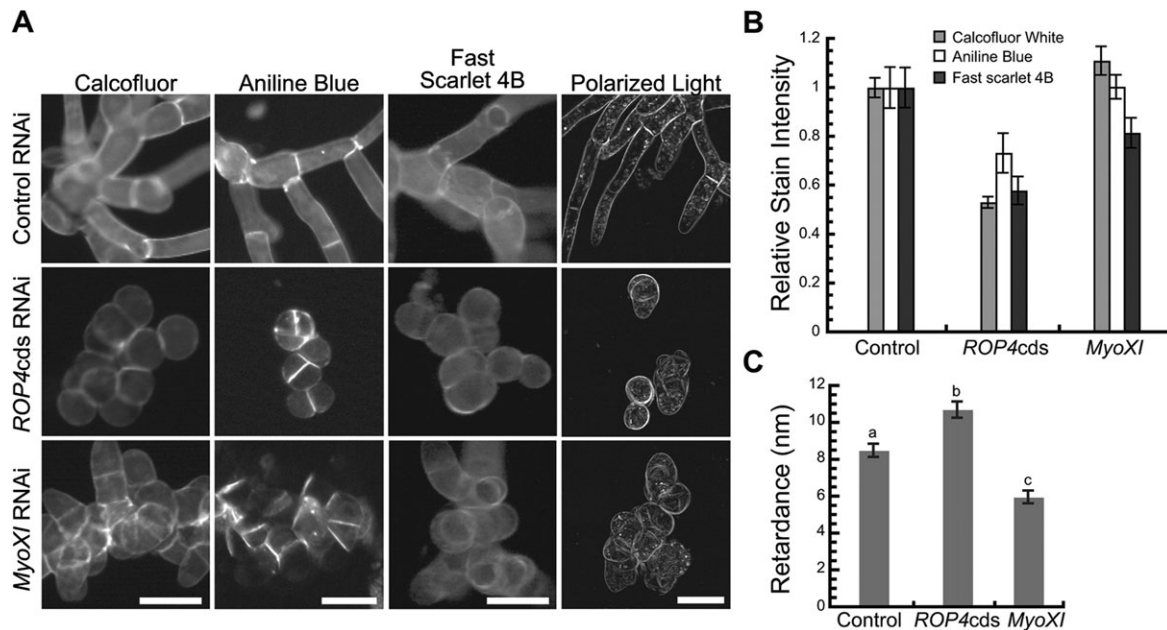


Fig. 4. Cell wall deposition is altered in *ROP* RNAi plants. (A) Micrographs of 7-day-old NLS4 plants expressing control, *ROP4cds* or *MyoXI* RNAi constructs that had been stained with Calcofluor, Aniline Blue and Fast Scarlet 4B or imaged with polarized light. Scale bars: 50 μ m. (B) Fluorescence intensity of Calcofluor (CW, gray), Aniline Blue (AB, white) and Fast Scarlet 4B (FS, dark gray) staining in plants expressing the indicated RNAi constructs normalized to that of 7-day-old NLS4 plants expressing the control construct [$n=60$ (CW), $n=15$ (AB) and $n=23$ (FS) plants], *ROP4cds* [$n=61$ (CW), $n=15$ (AB), $n=18$ (FS) plants] and *MyoXI* [$n=25$ (CW), $n=19$ (AB), $n=22$ (FS) plants]. (C) Light retardance of cell walls based on polarized-light images using three external cell walls from eight to ten images for each RNAi construct. Error bars represent s.e.m., and the letters above the bars indicate statistical groups with $\alpha=0.05$ using ANOVA.

of the ATG of *ROP1*, *ROP2* or *ROP3*). To ensure that ROP expression constructs produced protein, we transformed these constructs into protoplasts and assayed expression after 3 days, which is before regeneration and apparent lethality. Immunoblotting with an antibody specific for ROP-family proteins verified that, as expected, both of the UBI-*ROP3* and UBI-*ROP4* overexpression constructs dramatically increased ROP protein levels (Fig. 5A). Thus, in moss, tight control of ROP protein levels appears to be required for viability.

As an alternative complementation strategy, we generated a line where one of the ROP loci was insensitive to the *ROP*-3'Utr RNAi construct. Because deletion of *ROP4* had the least impact on the expression of the remaining ROP genes (Fig. 1B), we rendered the *ROP4* locus insensitive to the *ROP* 3'Utr RNAi construct by replacing its 3'-untranslated region with a hygromycin-resistance marker using homologous recombination (NLS4/*ROP4* Δ 3'Utr) (Fig. 5B). This alteration of the locus did not significantly impact plant area or solidity (supplementary material Fig. S2). As expected, transforming the RNAi-insensitive line with the *ROP4cds* RNAi construct, which targets the coding sequence, resulted in small unpolarized plants (Fig. 5B,C). By contrast, transforming the insensitive line with the *ROP*-3'Utr RNAi construct produced polarized plants (Fig. 5B). Although these plants had a solidity that was almost the same as that of control RNAi plants, they were only ~58% of the size (Fig. 5C). The amount of transcript from the modified *ROP4* locus was unaffected by expression of the *ROP*-3'Utr RNAi construct (Fig. 5D). Thus, plants expressing predominantly *ROP4* had polarized growth, but were significantly smaller, and their total transcript level of ROP genes was reduced, as compared with those of control RNAi plants.

Using homologous recombination to target the *ROP4* genomic locus, we were able to render *ROP4* insensitive to the RNAi construct. Using this strategy, we tested whether GFP-*ROP4* fusion

proteins could rescue polarized growth, and as a control we replaced the genomic coding sequence of *ROP4* with cDNA (supplementary material Fig. S3A). Surprisingly, we discovered that neither the *ROP4* cDNA nor the GFP-*ROP4* fusions were able to rescue polarized growth (supplementary material Fig. S3A), suggesting that maintaining the genomic intron and exon structure of *ROP4* is crucial for function. Taken together, our data suggest that *ROP4* is sufficient for polarized growth. However, total levels of ROP genes are tightly regulated, where even rather modest reductions in that level the reduce growth rate and higher levels kill the plant.

Silencing ROP genes stimulates actin dynamics

To investigate the molecular basis of the function of ROP proteins during growth, we analyzed the organization and dynamics of the actin and microtubule cytoskeletons. We imaged actin in the protonemal apical cells of plants expressing Lifeact-mEGFP (Vidali et al., 2009a) by using spinning-disc confocal microscopy. Similar to control plants, *ROP* RNAi plants had a meshwork of actin that mostly resided at the cell cortex. Control plants also tended to have filaments that were generally parallel to the long axis of the cell, whereas *ROP* RNAi cells tended to have a random orientation of filaments (Fig. 6A). To assay actin organization quantitatively, we attempted to use metrics that measured actin density (percent occupancy) and bundling (skewness). However, because the actin arrays were dense in the cell cortex, the thresholding and skeletonizing procedures failed to capture all filaments within the network. Instead, we used an analysis that measured the degree of orientation present in the image (Marga et al., 2005; Vidali et al., 2007). Briefly, fast Fourier transforms (FFT) were obtained for the images of Lifeact-mEGFP and fitted with an ellipse. The more orientational the order, the narrower and hence more eccentric the ellipse. Using this analysis, we confirmed that *ROP* RNAi cells had more disordered actin arrays compared with control cells (Fig. 6B).

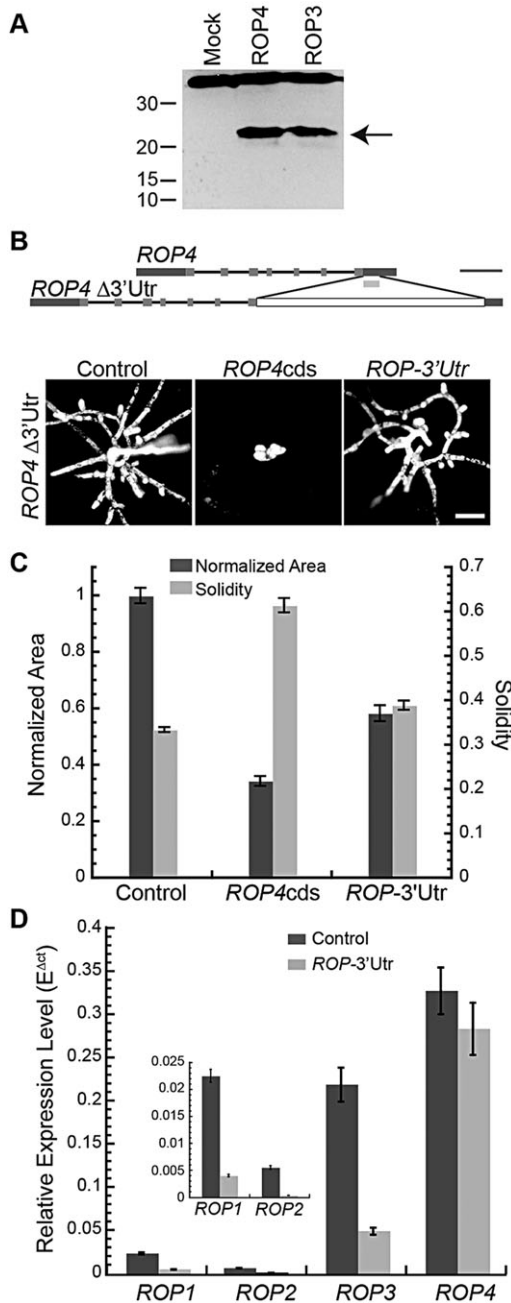


Fig. 5. A single ROP gene is sufficient for polarized growth.

(A) Immunoblot using an antibody against *A. thaliana* ROP2 shows a large increase in ROP protein level in protoplasts overexpressing ROP4 or ROP3. Arrow indicates position where moss ROP proteins migrate, at ~21 kDa. Upper band is a cross-reacting protein, demonstrating equal protein load on the gel. (B) Diagram illustrating the homologous-recombination-mediated replacement of the 3'UTR in the *ROP4* locus targeted by the *ROP-3'Utr* RNAi construct, generating a stable RNAi-insensitive line. Exons are indicated in light gray, introns in black, untranslated regions in dark gray and the hygromycin-resistance cassette in white. Scale bar: 500 bp. Below, micrographs of chlorophyll autofluorescence of 7-day-old NLS4/*ROP4Δ3'Utr* plants regenerated from protoplasts expressing the indicated RNAi constructs. Scale bar: 100 μ m. (C) Quantification of plant area (dark gray) and solidity (light gray) for control ($n=75$ plants), *ROP4cds* ($n=75$ plants) and *ROP-3'Utr* ($n=75$ plants). (D) Relative expression levels of ROP genes normalized to that of *UBIQUITIN10* in 8-day-old NLS4/*ROP4Δ3'Utr* plants expressing control (dark gray) and *ROP-3'Utr* (light gray) RNAi constructs. E is the amplification efficiency. Error bars represent s.e.m. Inset in D, relative expression levels of *ROP1* and *ROP2* normalized to that of *UBIQUITIN10*.

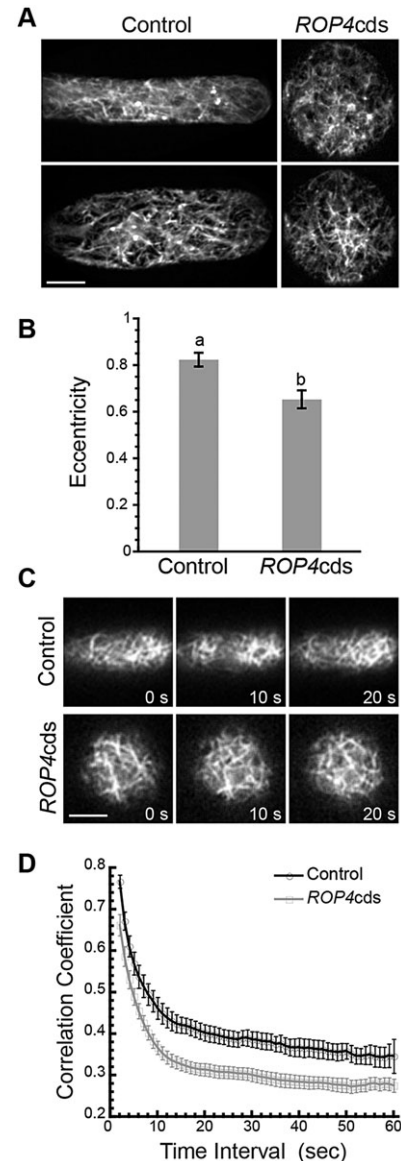


Fig. 6. ROP RNAi impacts on cortical actin dynamics and organization.

(A) Confocal images of single cortical planes through 6-day-old NLS4/Lifeact-mEGFP plants expressing either control or *ROP4cds* RNAi constructs. (B) Eccentricity measurements for 6-day-old NLS4/Lifeact-mEGFP plants expressing either control ($n=6$ cells) or *ROP4cds* ($n=9$ cells) RNAi constructs as a measurement of actin filament order. Error bars represent s.e.m., and letters above bars indicate statistical groups with $\alpha=0.05$ using ANOVA. (C) Spinning-disc confocal images of 6-day-old NLS4/Lifeact-mEGFP plants expressing either control or *ROP4cds* RNAi constructs. Cells were imaged at the cortical plane every second. Also see supplementary material Movie 1. (D) The correlation coefficient between two images was calculated at all possible temporal spacings (time interval) for time-lapse sequence acquisitions of 6-day-old NLS4/Lifeact-mEGFP plants expressing either control ($n=6$ cells) or *ROP4cds* ($n=8$ cells) RNAi constructs. Error bars represent s.e.m. Scale bars: 5 μ m.

This is similar to what has been measured previously for cells that lack actin-associated proteins, such as profilin, class-II formins and myosin XI (Vidali et al., 2007, 2009b, 2010).

To investigate whether, in addition to altering actin organization, ROP proteins impact actin dynamics, we imaged the cell cortex of apical cells in plants that expressed Lifeact-mEGFP once every second over the course of 1 minute by using spinning-disc confocal

microscopy. With these data, we quantified global changes in actin organization by calculating the correlation coefficient of the intensity of the Lifeact–mEGFP signal at all pixel locations between time points (Vidali et al., 2010). This analysis examines the degree of change in the images of Lifeact–mEGFP – a greater change between images results in a steeper decay of the correlation coefficient and indicates increased dynamics. Interestingly, *ROP* RNAi plants had a faster decay than that of control plants (Fig. 6C,D; supplementary material Movie 1), revealing that actin-filament dynamics were increased. This effect was not caused by cell rounding, as indicated by performing the same analysis for *MyoXI* RNAi plants, which were just as round as *ROP* RNAi plants but had actin dynamics that were indistinguishable from those of the wild type (Vidali et al., 2010). These data imply that in wild-type plants, ROP-family proteins function to suppress actin-filament dynamics.

Microtubule dynamics and organization are not specifically regulated by ROP

In *A. thaliana*, *AtROP6* and *AtROP11* have been linked to microtubule patterning, in the indentation regions of leaf pavement cells (Xu et al., 2010; Sorek et al., 2011) and during the formation of secondary cell walls in xylem cells (Oda and Fukuda, 2012). Thus, we investigated whether moss ROP proteins also impact the microtubule cytoskeleton. To image the microtubule cytoskeleton, we tagged one of the α -tubulin genes with mCherry, generating NLS4 plants expressing Lifeact–mEGFP and mCherry– α -tubulin (NLS4/Lifeact–mEGFP/mCherry– α -tubulin). Of note, altering this α -tubulin locus did not significantly impact plant growth or morphology (supplementary material Fig. S4).

After transformation, we imaged microtubules in protonemal apical cells (Fig. 7A; supplementary material Movie 2) and quantified dynamics using the same method as that used for actin.

The *ROP* RNAi plants exhibited substantially reduced microtubule dynamics as compared with that of control plants (Fig. 7B). To investigate whether this reduction was specific for loss of ROP-protein function, we measured microtubule dynamics in the *MyoXI* RNAi plants, which were similar in size and shape to *ROP* RNAi plants. In addition, we investigated the effect of altering actin dynamics by treating wild-type cells with 13 μ M latrunculin B and reducing microtubule dynamics through treatment with 50 μ M taxol. None of these treatments noticeably altered microtubule organization (Fig. 7A; supplementary material Movie 2), but all of them reduced microtubule dynamics – taxol and *MyoXI* RNAi inhibited dynamics to approximately the same extent as *ROP* RNAi, and latrunculin B inhibited dynamics even more (Fig. 7B).

To investigate the possibility that ROP proteins regulate a specific aspect of microtubule dynamics, we measured polymerization and depolymerization rates (Fig. 7C). As expected, both polymerization and depolymerization rates were significantly reduced with taxol, validating the assay. *ROP* RNAi had little, if any, effect on the depolymerization rate but reduced the rate of polymerization by approximately 24%. However, a similar reduction occurred in the *MyoXI* RNAi plants, and an even larger one in those treated with latrunculin B. These data show that the reduction in microtubule dynamics seen in the *ROP* RNAi plants is arguably a secondary effect, contingent upon the disruption of actin.

To determine whether loss of ROP proteins affects cortical microtubule architecture, we quantified both microtubule bundling ('skewness') and density ('occupancy') (Higaki et al., 2010). Although taxol significantly reduced microtubule density, presumably reflecting bundling, effects of the other treatments were small and scarcely significant (Fig. 7D), supporting the idea that, in moss, the behavior of cortical microtubules and ROP proteins are independent.

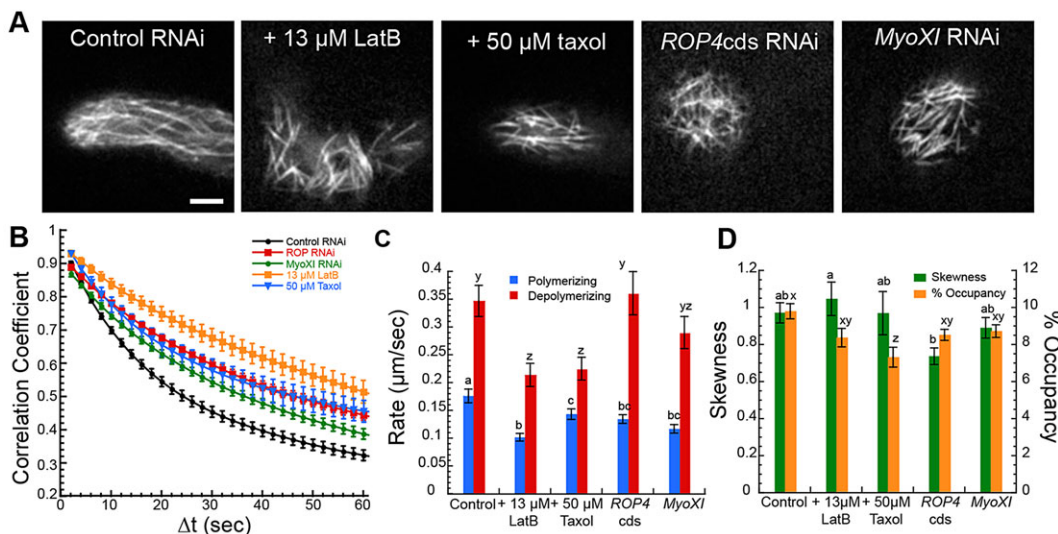


Fig. 7. *ROP* RNAi impacts cortical microtubule dynamics and organization. Also see supplementary material Movie 2. (A) Confocal images of single cortical planes through 6-day-old NLS4/Lifeact–mEGFP/mCherry– α -tubulin plants expressing control, *ROP4cds* and *MyoXI* RNAi constructs, as well as control RNAi plants treated with 13 μ M latrunculin B (LatB) or 50 μ M taxol. Scale bar: 5 μ m. (B) The correlation coefficient between two images was calculated at all possible temporal spacings (time interval) for time-lapse sequence acquisitions of control ($n=44$ cells, black circles), control cells treated with either 13 μ M LatB ($n=10$ cells, orange squares) or 50 μ M taxol ($n=10$ cells, blue triangles), *ROP4cds* ($n=30$ cells, red squares) and *MyoXI* ($n=27$ cells, green circles). (C) Quantification of microtubule polymerization (blue) and depolymerization (red) rates. For each condition in B, 12–15 elongating and 12–15 shrinking microtubules were measured. Error bars represent s.e.m., and letters above bars indicate statistical groups with $\alpha=0.05$ using ANOVA. (D) Skewness and filament density measurements of 6-day-old NLS4/Lifeact–mEGFP/mCherry– α -tubulin plants expressing control ($n=15$ cells), *ROP4cds* ($n=15$ cells) and *MyoXI* ($n=11$ cells) RNAi constructs in addition to control RNAi plants treated with either 13 μ M LatB ($n=10$ cells) or 50 μ M taxol ($n=10$ cells). Error bars represent s.e.m., and letters above bars indicate statistical groups with $\alpha=0.05$ using ANOVA.

DISCUSSION

Capitalizing on the fact that the moss *Physcomitrella patens* has but four ROP genes, we have developed a system in which a loss of ROP-protein function can be studied informatively, and we have used this system to characterize the function of ROP-family members in cell shape, growth rate and cytoskeletal dynamics. We show that this family helps maintain growth rate and cell adhesion, suppress actin dynamics and are essential for cells to become polarized.

Here, we show that ROP proteins are essential for tip growth in moss, in so far as silencing of the four ROP genes yielded plants comprising unpolarized cells. We also show that single-gene-knockout lines for each of the four moss ROP genes were capable of tip growth but were also reduced in size. Likewise, when three of the four ROP genes were silenced in a stable line expressing an RNAi-insensitive allele of *ROP4*, smaller but polarized plants resulted. These findings suggest that, in addition to an essential role in cell polarity, all four family members contribute to maintaining the growth rate. Interestingly, knocking out any single ROP gene reduced the expression of the three remaining loci, and the total expression of ROP genes correlated inversely with plant size, suggesting that the transcript levels of ROP genes, and hence presumably protein level, exert a nearly quantitative effect on growth rate. These unusual interactions between ROP loci suggest that the transcript levels of ROP genes are tightly regulated. Consistent with this, it was not possible to regenerate plants when ROP genes were overexpressed, even under their own promoters, implying that excess amounts of ROP proteins are toxic, supporting the case for strict control over transcript abundance.

It is widely accepted that, for plants, the ROP-family proteins are essential for polarizing the cell, as shown here. However, this acceptance is based to a large extent on the overexpression of ROP isoforms causing tip-growing cells to swell apically, indicative of a loss of polarity (Li et al., 1999; Molendijk et al., 2001; Jones et al., 2002). Indeed, a similar phenotype has been observed recently for moss protonema when overexpression of a ROP protein was induced in polarized cells (Ito et al., 2014). But if a protein helps to specify cell polarity, then, logically, an excess of that protein should increase cell polarization, not the reverse. Although frequently ignored, pitfalls of overexpression are manifold, as eloquently reviewed by Gibson et al. (2013). As appears to be true for ROP genes in moss, the control of expression rather than functional specialization might frequently account for the fitness of a gene family.

Albeit mainly through overexpression, activity of the ROP family has been linked in seed plants to the organization of actin and has been implicated in promoting actin filament assembly (Fu et al., 2001, 2002). From these studies, it is expected that loss of function of ROP-family proteins leads to a decrease in actin filament assembly, resulting in less filamentous actin. However, we found that filament density was not detectably decreased in the *ROP* RNAi plants, suggesting that the activity of ROP proteins might not directly promote actin polymerization. Because, to our knowledge, actin dynamics have not been previously quantified in studies of the plant ROP family, it is unknown whether the reported activation of ROP proteins increased polymerization directly or, instead, suppressed turnover, leading to a net increase in filament density. Our data quantify actin dynamics in cells in which the function of ROP proteins was drastically reduced, thereby giving mechanistic insights into the effect of ROPs on the actin cytoskeleton. Surprisingly, in *ROP* RNAi plants, actin organization changed faster (on a time scale of seconds) than it did in controls. These data

implicate ROP-family members as actin stabilizers. This might occur by activating actin-stabilizing factors, such as bundlers, or by inhibiting actin depolymerization factors, such as actin depolymerizing factor (ADF)/cofilin-family members and actin interacting protein 1 (AIP1). We hypothesize that negative regulation of actin dynamics is an ancestral function of the ROP GTPase.

ROP RNAi plants are unpolarized, but still have dynamic actin filaments, a phenotype similar to that observed for *MyoXI* RNAi plants (Vidali et al., 2010). This behavior is distinct from that occurring with loss of function of ADF or AIP1, where cells are defective in cell polarity and actin filaments hardly move (Augustine et al., 2008, 2011), or with actin-depolymerizing agents that remove actin filaments (Harries et al., 2005). Thus, dynamic actin is necessary but not sufficient for cell polarization.

In angiosperms, ROP proteins have been localized by means of immunocytochemistry to the apical cell membrane in both pollen tubes (Lin et al., 1996) and root hairs (Molendijk et al., 2001). In both of these cell types, GFP-tagged ROP proteins localize in a similar manner (Li et al., 1999; Jones et al., 2002). Although we were unable to demonstrate that GFP-tagged ROPs are functional in moss, we found that they labeled the apical membrane in tip-growing protonemata (supplementary material Fig. S3B). Therefore, we posit that ROP proteins polarize the cell by stabilizing a spatially restricted subset of actin filaments at the site of polarized secretion.

In *A. thaliana*, various ROP proteins, in addition to being linked to actin, have been linked to the microtubule cytoskeleton. In moss, *ROP* RNAi plants indeed had reduced microtubule dynamics, so did plants with similar cell sizes and shapes. Furthermore, the strongest suppression of microtubule dynamics was caused by eliminating actin with latrunculin B. This suggests that microtubule dynamics are inhibited as a general consequence of unpolarized growth or perhaps in response to an altered actin cytoskeleton. Interplay between these two cytoskeletons has been observed previously, where recovery of one cytoskeleton after depolymerization depends on the presence of the other (Sampathkumar et al., 2011). It would be interesting to examine the impact of oryzalin or taxol on actin dynamics and organization to determine whether this codependency also exists in moss.

We were surprised to discover that *ROP* RNAi plants, in addition to being unable to initiate tip growth, were defective in cellular adhesion. The plants that had been subjected to RNAi broke apart readily into single cells or small clumps when manipulated with a fine needle, or when exposed to mild sonication. Extensive cell separation, strikingly similar to that of *ROP* RNAi plants, has also been reported recently for *P. patens* lines that are defective in enzymes for prenylation (Thole et al., 2014). Given that a ROP protein must be prenylated to be recruited to the membrane, loss of cell polarity and cell separation in the prenylation mutants are arguably caused by the loss of ROP activity.

A cell adhesion phenotype specifically has not been reported in previous studies of ROP function in seed plants; however, a number of mutations either in ROP genes or ROP effectors lead to gaps between cells in the epidermis. For example, perturbation of *AtROP2* and *AtROP6* activity leads to malformed lobes in leaf pavement cells and to occasional gaps between cells (Xu et al., 2010). Mutants of *SPK1*, one of the known ROP guanine-nucleotide exchange factors in *A. thaliana*, have similarly gapped pavement cells, especially immediately around guard cells (Basu, et al., 2008). Pirogi interacts with active *AtROP2* to positively regulate the Arp2/3 complex; *pirogi* mutants, as well as a number of mutations of the

Arp2/3 complex and activators of the Arp2/3 complex, also have gaps between adjacent pavement cells and cell adhesion defects in etiolated hypocotyls (Basu et al., 2004, 2005; El-Din El-Assal et al., 2004; Kotchoni et al., 2009). The appearance of gaps in leaf epidermis has been interpreted both in terms of lobe malformation and decreased cell adhesion.

In our investigation of cell adhesion, Ca²⁺-mediated effects were undetectable, suggesting that if pectic Ca²⁺ cross-bridges are crucial for cell adhesion in moss protonemata, then they are unusually inaccessible to the medium. Curiously, the pectin polymer that bears Ca²⁺ cross-bridges, homo-galacturonan, is recalcitrant to extraction through Ca²⁺ chelation in the gametophores of *P. patens* (Domozych et al., 2014) and of *Selaginella moellendorffii* (Harholt et al., 2012) but apparently not in *P. Patens* protonemata (Moller et al., 2007). When stained with fluorophores specific for cellulose, the intensity in *ROP* RNAi cell walls was low compared with that of control or *MyoXI* RNAi plants, suggesting that cellulose is present in reduced amounts in the absence of ROP proteins. However, in the cell walls of *ROP* RNAi plants, birefringent retardance actually increased. Although changes in microfibril organization cannot be excluded entirely, the increased retardation in these plants is mostly likely to be an optical consequence of their increased diameter; and therefore, the lowered intensity of staining of the dyes can be taken to indicate a change in cell wall composition or structure, limiting cellulose accessibility. Be that as it may, the reduced dye staining and cell adhesion show that ROPs have a role in assembling the cell wall.

Interestingly, although the cell walls of *ROP* RNAi plants had increased retardance compared with those of control plants, *MyoXI* RNAi cell walls had a notably decreased retardance, even though they are similar in size and shape to *ROP* RNAi plants. Given that the rate of cellulose synthesis in *A. thaliana* is sensitive to the rate of vesicle secretion (McFarlane et al., 2014), the lowered retardance of the *MyoXI* RNAi cell walls is fully consistent with myosin XI sustaining secretion in tip-growing cells, as widely proposed (Cai et al., 2015). By the same token, the increased retardance of the *ROP* RNAi cell walls argues against ROP proteins having a role in governing the rate of exocytosis. Instead, ROP-family proteins might restrict vesicle delivery or fusion to specific sites on the membrane, defining or enforcing the apical domain. In the absence of this localizing activity, secretion would be random yet undiminished, plausibly distorting cell wall deposition and assembly, and leading to the observed isotropic expansion and defective cell adhesion.

MATERIALS AND METHODS

Moss tissue culture, protoplast transformation and imaging

Moss tissue culture and protoplast transformations were performed as previously described (Vidali et al., 2007). Plants were imaged and analyzed morphometrically at 6 to 8 days after transformation, as previously described (Vidali et al., 2007).

qRT-PCR analysis

At 8 days of age, 200–1000 plants in which the indicated genes had been silenced were manually picked with a fine needle, and RNA extraction, cDNA synthesis and qRT-PCR were performed as previously described (Vidali et al., 2010) with the modifications described as follows. The cDNA was synthesized from total RNA using SuperScript III reverse transcriptase (Invitrogen, Carlsbad, CA) and oligo-dT, following the manufacturer's protocol, except for the elution volume, which was reduced from 50 µl to 25 µl. All qRT-PCR reactions used 2–20 ng of cDNA template in a 12.5 µl reaction using the Brilliant II SYBR green QPCR master mix (Agilent Technologies, Santa Clara, CA). The PCR conditions were as follows – 95°C

for 10 min, followed by 40 cycles of 95°C for 30 s and 60°C for 1 min, and ending with a melting curve analysis. Amplification efficiency for each set of primers (supplementary material Table S1) was calculated from standard curves, and these efficiencies were used in the calculation of the relative expression levels.

Generation of *ROP* RNAi and expression constructs

The sequences used for the RNAi constructs were amplified from *P. patens* cDNA using appropriate primers (supplementary material Table S1). For constructs containing sequences from more than one gene, the individual PCR products were fused by using restriction digest and ligation, as previously described (Vidali et al., 2007). The resulting fused sequences were then re-amplified by using PCR. PCR fragments were cloned into pENTR/D-TOPO (Invitrogen), and resulting plasmids were verified by sequencing. The RNAi fragments were then inserted into the destination RNAi expression vector pUGGi (Bezanilla et al., 2005) using LR clonase (Invitrogen) reactions.

Expression constructs were amplified from moss cDNA and cloned into pENTR/D-TOPO (Invitrogen) using appropriate primers (supplementary material Table S1). After verification by sequencing, LR clonase (Invitrogen) reactions were used to transfer the expression sequences to pTHubiGate (Vidali et al., 2007).

Generation of moss stable lines

The constructs used to make stable lines were generated by using multisite Gateway recombination (Invitrogen) and transformed into moss, as previously described (Vidali et al., 2007). To delete a region of a ROP genomic locus, sequences immediately upstream and downstream of the region to be replaced [either the entire gene (*Δrop1–Δrop4*) or the 3'UTR (*Δrop1–Δrop4*)] were amplified and cloned into pDONR-P1P4 and pDONR-P3P2, respectively, using BP clonase II reactions (Invitrogen). These targeting sequences were recombined with L4L3 nos-lox-hygro-lox using a LR Clonase II plus reaction (Invitrogen). Linearized deletion constructs used for transformation were generated by either PCR (*Δrop1–Δrop4*) or digestion of the restriction sites (*ROP4Δ3*'Utr) flanking the targeting sequences.

To generate stable lines expressing GFP-tagged *ROP4*, the *ROP4* coding sequence was amplified with appropriate primers (supplementary material Table S1) from moss cDNA, and cloned into pENTR/D-TOPO (Invitrogen). After sequencing, the coding sequence was then isolated using the restriction sites *AscI* and *SpeI*, and inserted into L5L4-mEGFP-*AscI*-*SpeI* or L5L4-3×mEGFP-*AscI*-*SpeI* plasmids, which results in an in-frame fusion of the ROP sequence with mEGFP or 3×mEGFP, generating L5L4-mEGFP-*ROP4*cds and L5L4-3×mEGFP-*ROP4*cds, respectively. A non-tagged version of the *ROP4*cds was also constructed (L5L4-*ROP4*cds). The 5' targeting sequence was amplified from genomic DNA and cloned into pDONR-P1P5r using BP Clonase II (Invitrogen), generating L1L5-*ROP4*-5'tarm. Similarly, the 3' targeting sequence was amplified and cloned into pDONR-P3P2 using BP Clonase II (Invitrogen), generating L3L2-*ROP4*-3'tarm. The L1L5-*ROP4*-5'tarm, L5L4-mEGFP-*ROP4*cds/L5L4-3×mEGFP-*ROP4*cds/L5L4-*ROP4*cds and L3L2-*ROP4*-3'tarm were recombined with L4L3 nos-lox-hygro-lox using LR Clonase II plus (Invitrogen) to generate the final constructs for homologous recombination in moss, mEGFP-*ROP4*cds-AR, 3×mEGFP-*ROP4*cds-AR and *ROP4*cds-AR.

The coding sequence of moss α-tubulin (Pp1s215_51V6 locus) was amplified from moss cDNA with appropriate primers (supplementary material Table S1) and cloned into pENTR/D-TOPO (Invitrogen). After verification by sequencing, the coding sequence was isolated with an *AscI* and *SpeI* restriction digest, and subsequently inserted into the L5L4-mCherry-*AscI*-*SpeI* plasmid generating L5L4-mCherry-α-tub215-51-1. Sequences upstream and downstream of the locus were amplified as targeting sequences for homologous recombination. The 5' targeting sequence was amplified and cloned into pDONR-P1P5r using BP Clonase II (Invitrogen), generating L1L5-α-tub215-51-1-5'tarm. Similarly, the 3' targeting sequence was amplified and cloned into pDONR-P3P2 using BP Clonase II (Invitrogen), generating L3L2-α-tub215-51-1-3'tarm. The L1L5-α-tub215-51-1-5'tarm, L5L4-mCherry-α-tub215-51-1 and L3L2-α-tub215-51-1-3'tarm were recombined with L4L3 nos-lox-hygro-lox using

LR Clonase II plus (Invitrogen) to generate the final construct for homologous recombination in moss, mCherry- α -tub215-51-1AR.

In all cases, proper targeting was verified by using PCR of genomic DNA from the stable lines using appropriate primers (supplementary material Table S1). Growth assays of stable lines were performed by imaging and analysis of 7-day-old regenerated protoplasts.

Generation of zeocin-resistant RNAi constructs

Zeocin-resistant RNAi constructs were constructed in order to transform the NLS4/*ROP4* Δ 3'Utr stable line, which is resistant to hygromycin. Briefly, a plasmid (pUBI-Nos) containing a cassette comprising the maize ubiquitin promoter, a multiple cloning site and a NOS terminator was linearized with *Sma*I, which cut in the multiple cloning site. The region containing inverted repeats was isolated from the control (pUGi), *ROP4*cds (pUG*ROP4*cdsi), *ROP* 3'Utr (pUG*ROP3*'Uti) and the RNAi destination vector (pUGGi) using a *Sac*I and *Kpn*I restriction digest. All fragments were blunted and ligated into the *Sma*I-linearized pUBI-Nos. The resulting plasmids were digested with *Bgl*II and *Hpa*I to isolate the maize ubiquitin promoter, inverted repeats and the NOS terminator. All fragments were then blunted and ligated into a pZeo vector (Perroud and Quatrano, 2008), generating pZUGi, pZUG*ROP4*cdsi, pZUG*ROP3*'Uti and pZUGGi.

Confocal microscopy

Regenerating plants were mounted on slides, as described previously (Vidali et al., 2009b). Slides were imaged on an inverted microscope (model Ti-E; Nikon Instruments, Melville, NY) that was equipped with a spinning-disc head (model CSU-X1; Yokogawa Corporation of America, Sugar Land, TX) and a 512 \times 512 electron multiplying CCD camera (iXON; Andor Technology, South Windsor, CT). Images were collected with a 1.4 NA 60 \times oil immersion objective (Nikon) at room temperature. Laser power and exposure times varied depending on what fusion protein was imaged, but were kept consistent within experiments. The image acquisition process was controlled by MetaMorph software (Molecular Devices, Sunnyvale, CA) and images were further processed with ImageJ, as described for specific analyses.

Localization of ROP proteins was determined in the stable line NLS4/mEGFP-*ROP4*cds. Five to ten slices from the apical dome were collected at 1- μ m intervals. Maximal projections were subsequently created in ImageJ. To increase visibility, enhance contrast and subtract background functions were applied to the images.

Quantification of cytoskeletal dynamics and organization

Correlation coefficient analysis of cytoskeletal dynamics was performed as previously described using a custom MATLAB function corr2 (Vidali et al., 2010). The resulting averaged correlation coefficients were plotted as a function of time and compared among treatments.

Confocal images of microtubules were manually thresholded, skeletonized and binarized before being converted into masks. These masks were then applied to the original images. The skewness macro (ImageJ) (Higaki et al., 2010) measures the distribution of the intensity of the filament pixels and reflects the relative degree of filament bundling. The filament density is given as the percentage of the total cell area in the focal plane that is occupied by the filament mask. Microtubule polymerization and depolymerization rates were measured by identifying the tip of a growing microtubule and measuring the displacement over time (8–18 s).

Actin filament organization using fast Fourier transform analysis was performed as previously described (Vidali et al., 2007) with modifications described as follows. Single-plane confocal images of filamentous actin were used instead of maximal projections from z-stacks. The average of the final three eccentricity values was used as the eccentricity value for the image.

Polarized-light microscopy and analysis

Plants were imaged on an Interphako polarized-light microscope (Carl Zeiss Microscopy LLC, Thornwood, NY) that was equipped with an LC Polscope quantification system (Cambridge Research Instruments, Woburn, MA) implementing the Universal Compensator (Oldenbourg and Mei, 1995). This system generates an image in which the intensity of each pixel is proportional to birefringent retardance. Because the system uses circularly

polarized light, the retardance data are independent of sample orientation. Retardance was quantified by taking the peak intensities of line scans across the cells by using ImageJ. Three to five cell walls were analyzed per image, and seven to ten images per condition were examined. The peak intensities are proportional to retardance with a gray level of 255=15 nm. Retardance values for each condition were then averaged and plotted.

Staining of the cell wall

At 1 week old, plants that had been regenerated from protoplasts were incubated in 1 ml of stain [10 μ g/ml Calcofluor White (fluorescent brightener 28, Sigma), 1% Aniline Blue or 100 μ g/ml Fast Scarlet 4B] for 30 min. All stain was removed, and plants were washed three times with water. Calcofluor-White- and Aniline-Blue-stained plants were mounted on a slide, and images of the plants that had been subjected to RNAi were captured as 24-bit RGB images with a 5 \times lens at 30 \times zoom on a fluorescence stereomicroscope [Leica MZ16FA (Leica Microsystems, Buffalo Grove, IL)] that was equipped with a color camera (Leica DF300FX) and either UV (for Calcofluor and Aniline Blue staining) or GFP2 (to identify gene-silenced plants) filter sets (Leica). Fast-Scarlet-4B-stained plants were mounted and imaged as described above for confocal microscopy. The fluorescence intensity of both the plant and a nearby background spot were measured in a 100 \times 100-pixel² region of the image using ImageJ. After background subtraction, the intensity values were averaged and plotted.

Sonication assay

Gene-silenced plants were transferred from selection plates to a 0.1-ml drop of water in the middle of a 3.5-cm petri dish. The dish was placed on the surface of a sonicating water bath (Sonicor, Ladd Research Industries, Williston, VT) that had been filled with 500 ml of water at power level 2 for 10 s. Plants were imaged before and after sonication using an epifluorescence stereomicroscope (Leica MZ16FA) that was equipped with a CCD camera (Leica DF300FX) with a GFP2 filter (Leica) to capture chlorophyll autofluorescence. The frequency of plant breakage was determined for each treatment.

Immunoblotting

To verify the expression of ROP proteins, moss protoplasts were transformed and processed for immunoblotting, as described previously (van Gisbergen et al., 2012). Immunoblotting was performed with a rabbit anti-*AtROP2* serum (Zhang et al., 2010). Chemiluminescence emission from horseradish peroxidase fused to a polyclonal goat anti-rabbit IgG secondary antibody (Jackson ImmunoResearch Laboratories, West Grove, PA) was detected on a gel doc system equipped for chemiluminescence detection (Bio-Rad laboratories, Hercules, CA).

Acknowledgements

We thank Luis Vidali, Peter van Gisbergen, Katherine Walsh and Alexis Tomaszewski for their technical support, and we are particularly grateful to Dan Szymanski (Purdue University) for providing antibodies against *AtROP2*.

Competing interests

The authors declare no competing or financial interests.

Author contributions

G.M.B. performed the majority of the experiments, supervised by M.B. T.I.B. performed polarized-light microscopy, and M.B. performed selected experiments. G.M.B., T.I.B. and M.B. wrote the paper.

Funding

This work was supported by the National Science Foundation [grant MCB-0747231 to M.B.]; and the David and Lucille Packard Foundation (to M.B.). G.M.B. was supported by the Gilgut Fellowship and the Plant Biology Graduate Program at the University of Massachusetts. The work on cellulose organization in the Baskin lab is supported by the Division of Chemical Sciences, Geosciences and Biosciences, Office of Basic Energy Sciences of the U.S. Department of Energy [grant DE-FG-03ER15421].

Supplementary material

Supplementary material available online at <http://jcs.biologists.org/lookup/suppl/doi:10.1242/jcs.172445/-/DC1>

References

- Augustine, R. C., Vidali, L., Kleinman, K. P. and Bezanilla, M. (2008). Actin depolymerizing factor is essential for viability in plants, and its phosphoregulation is important for tip growth. *Plant J.* **54**, 863-875.
- Augustine, R. C., Pattavina, K. A., Tüzel, E., Vidali, L. and Bezanilla, M. (2011). Actin interacting protein1 and actin depolymerizing factor drive rapid actin dynamics in *Physcomitrella patens*. *Plant Cell*. **23**, 3696-3710.
- Basu, D., El-Din El-Assal, S., Le, J., Mallery, E. L. and Szymanski, D. B. (2004). Interchangeable functions of Arabidopsis PIROGI and the human WAVE complex subunit SRA1 during leaf epidermal development. *Development* **131**, 4345-4355.
- Basu, D., Le, J., El-Din El-Assal, S., Huang, S., Zhang, C., Mallery, E. L., Koliantz, G., Staiger, C. J. and Szymanski, D. B. (2005). DISTORTED3/SCAR2 is a putative Arabidopsis WAVE complex subunit that activates the Arp2/3 complex and is required for epidermal morphogenesis. *Plant Cell* **17**, 502-524.
- Basu, D., Le, J., Zakharova, T., Mallery, E. L. and Szymanski, D. B. (2008). A SPIKE1 signaling complex controls actin-dependent cell morphogenesis through the heteromeric WAVE and ARP2/3 complexes. *Proc. Natl. Acad. Sci. USA* **105**, 4044-4049.
- Bezanilla, M., Perroud, P.-F., Pan, A., Klueh, P. and Quatrano, R. S. (2005). An RNAi system in *Physcomitrella patens* with an internal marker for silencing allows for rapid identification of loss of function phenotypes. *Plant Biol.* **7**, 251-257.
- Brembu, T., Winge, P. and Bones, A. M. (2005). The small GTPase AIRAC2/ROP7 is specifically expressed during late stages of xylem differentiation in Arabidopsis. *J. Exp. Bot.* **56**, 2465-2476.
- Cai, G., Parrotta, L. and Cresti, M. (2015). Organelle trafficking, the cytoskeleton, and pollen tube growth. *J. Integr. Plant Biol.* **57**, 63-78.
- Camacho, L. and Malhó, R. (2003). Endo/exocytosis in the pollen tube apex is differentially regulated by Ca²⁺ and GTPases. *J. Exp. Bot.* **54**, 83-92.
- Craddock, C., Lavagi, I. and Yang, Z. (2012). New insights into Rho signaling from plant ROP/Rac GTPases. *Trends Cell Biol.* **22**, 492-501.
- Domozych, D. S., Sørensen, I., Popper, Z. A., Ochs, J., Andreas, A., Fangel, J. U., Pielach, A., Sacks, C., Brechka, H., Ruisi-Besares, P. et al. (2014). Pectin metabolism and assembly in the cell wall of the charophyte green alga *Penium margaritaceum*. *Plant Physiol.* **165**, 105-118.
- Eklund, D. M., Svensson, E. M. and Kost, B. (2010). *Physcomitrella patens*: a model to investigate the role of RAC/ROP GTPase signalling in tip growth. *J. Exp. Bot.* **61**, 1917-1937.
- El-Din El-Assal, S., Le, J., Basu, D., Mallery, E. L. and Szymanski, D. B. (2004). DISTORTED2 encodes an ARPC2 subunit of the putative Arabidopsis ARP2/3 complex. *Plant J.* **38**, 526-538.
- Foucart, C., Jauneau, A., Gion, J.-M., Amelot, N., Martinez, Y., Panegos, P., Grima-Pettenati, J. and Sivadon, P. (2009). Overexpression of Eg ROP1, a Eucalyptus vascular-expressed Rac-like small GTPase, affects secondary xylem formation in Arabidopsis thaliana. *New Phytol.* **183**, 1014-1029.
- Fowler, J. E. (2010). Evolution of the ROP GTPase signaling module. In *Integrated G Protein Signaling in Plants*, 1st edn. (ed. S. Yalovsky, R. Baluska and A. Jones), pp. 305-327. Berlin; Heidelberg: Springer-Verlag.
- Fu, Y., Wu, G. and Yang, Z. (2001). ROP GTPase-dependent dynamics of tip-localized F-actin controls tip growth in pollen tubes. *J. Cell Biol.* **152**, 1019-1032.
- Fu, Y., Li, H. and Yang, Z. (2002). The ROP2 GTPase controls the formation of cortical fine F-actin and the early phase of directional cell expansion during Arabidopsis organogenesis. *Plant Cell* **14**, 777-794.
- Gibson, T. J., Seiler, M. and Veitia, R. A. (2013). The transience of transient overexpression. *Nat. Methods* **10**, 715-721.
- Gu, Y., Fu, Y., Dowd, P., Li, S., Vernoud, V., Gilroy, S. and Yang, Z. (2005). A Rho family GTPase controls actin dynamics and tip growth via two counteracting downstream pathways in pollen tubes. *J. Cell Biol.* **169**, 127-138.
- Gu, Y., Li, S., Lord, E. M. and Yang, Z. (2006). Members of a novel class of Arabidopsis Rho guanine nucleotide exchange factors control Rho GTPase-dependent polar growth. *Plant Cell* **18**, 366-381.
- Harholt, J., Sørensen, I., Fangel, J., Roberts, A., Willats, W. G. T., Scheller, H. V., Petersen, B. L., Banks, J. A. and Ulvskov, P. (2012). The glycosyltransferase repertoire of the spikemoss *Selaginella moellendorffii* and a comparative study of its cell wall. *PLoS ONE* **7**, e35846.
- Harries, P. A., Pan, A. and Quatrano, R. S. (2005). Actin-related protein2/3 complex component ARPC1 is required for proper cell morphogenesis and polarized cell growth in *Physcomitrella patens*. *Plant Cell* **17**, 2327-2339.
- Hepler, P. K. (2005). Calcium: a central regulator of plant growth and development. *Plant Cell* **17**, 2142-2155.
- Higaki, T., Kutsuna, N., Sano, T., Kondo, N. and Hasezawa, S. (2010). Quantification and cluster analysis of actin cytoskeletal structures in plant cells: role of actin bundling in stomatal movement during diurnal cycles in Arabidopsis guard cells. *Plant J.* **61**, 156-165.
- Ito, K., Ren, J. and Fujita, T. (2014). Conserved function of Rho-related ROP/RAC GTPase signaling in regulation of cell polarity in *Physcomitrella patens*. *Gene* **544**, 241-247.
- Jones, M. A., Shen, J.-J., Fu, Y., Li, H., Yang, Z. and Grierson, C. S. (2002). The Arabidopsis Rop2 GTPase is a positive regulator of both root hair initiation and tip growth. *Plant Cell* **14**, 763-776.
- Kotchoni, S. O., Zakharova, T., Mallery, E. L., Le, J., El-Din El-Assal, S. and Szymanski, D. B. (2009). The association of the Arabidopsis actin-related protein2/3 complex with cell membranes is linked to its assembly status but not its activation. *Plant Physiol.* **151**, 2095-2109.
- Li, H., Lin, Y., Heath, R. M., Zhu, M. X. and Yang, Z. (1999). Control of pollen tube tip growth by a Rop GTPase-dependent pathway that leads to tip-localized calcium influx. *Plant Cell* **11**, 1731-1742.
- Lin, Y. and Yang, Z. (1997). Inhibition of pollen tube elongation by micro-injected anti-ROP1Ps antibodies suggests a crucial role for Rho-type GTPases in the control of tip growth. *Plant Cell* **9**, 1647-1659.
- Lin, Y., Wang, Y., Zhu, J. K. and Yang, Z. (1996). Localization of a Rho GTPase implies a role in tip growth and movement of the generative cell in pollen tubes. *Plant Cell* **8**, 292-303.
- Lin, D., Nagawa, S., Chen, J., Cao, L., Chen, X., Xu, T., Li, H., Dhonskhe, P., Yamamuro, C., Friml, J. et al. (2012). A ROP GTPase-dependent auxin signaling pathway regulates the subcellular distribution of PIN2 in Arabidopsis roots. *Curr. Biol.* **22**, 1319-1325.
- Lin, D., Ren, H. and Fu, Y. (2015). ROP GTPase-mediated auxin signaling regulates pavement cell interdigitation in Arabidopsis thaliana. *J. Integr. Plant Biol.* **57**, 31-39.
- Lord, E. M. and Mollet, J.-C. (2002). Plant cell adhesion: a bioassay facilitates discovery of the first pectin biosynthetic gene. *Proc. Natl. Acad. Sci. USA* **99**, 15843-15845.
- Marga, F., Grandbois, M., Cosgrove, D. J. and Baskin, T. I. (2005). Cell wall extension results in the coordinate separation of parallel microfibrils: evidence from scanning electron microscopy and atomic force microscopy. *Plant J.* **43**, 181-190.
- McFarlane, H. E., Döring, A. and Persson, S. (2014). The cell biology of cellulose synthesis. *Annu. Rev. Plant Biol.* **65**, 69-94.
- Mizuta, Y. and Higashiyama, T. (2014). Antisense gene inhibition by phosphorothioate antisense oligonucleotide in Arabidopsis pollen tubes. *Plant J.* **78**, 516-526.
- Molendijk, A. J., Bischoff, F., Rajendrakumar, C. S. V., Friml, J., Braun, M., Gilroy, S. and Palme, K. (2001). Arabidopsis thaliana Rop GTPases are localized to tips of root hairs and control polar growth. *EMBO J.* **20**, 2779-2788.
- Moller, I., Sørensen, I., Bernal, A. J., Blaukopf, C., Lee, K., Øbro, J., Pettolino, F., Roberts, A., Mikkelsen, J. D., Knox, J. P. et al. (2007). High-throughput mapping of cell-wall polymers within and between plants using novel microarrays. *Plant J.* **50**, 1118-1128.
- Oda, Y. and Fukuda, H. (2012). Initiation of cell wall pattern by a Rho- and microtubule-driven symmetry breaking. *Science* **337**, 1333-1336.
- Oldenbourg, R. and Mei, G. (1995). New polarized light microscope with precision universal compensator. *J. Microsc.* **180**, 140-147.
- Perroud, P. F. and Quatrano, R. S. (2008). BRICK1 is required for apical cell growth in filaments of the moss *Physcomitrella patens* but not for gametophore morphology. *Plant Cell*. **20**, 411-422.
- Roberts, A. W., Roberts, E. M. and Haigler, C. H. (2012). Moss cell walls: structure and biosynthesis. *Front. Plant Sci.* **3**, 166.
- Sampathkumar, A., Lindeboom, J. J., Debolt, S., Gutierrez, R., Ehrhardt, D. W., Ketelaar, T. and Persson, S. (2011). Live cell imaging reveals structural associations between the actin and microtubule cytoskeleton in Arabidopsis. *Plant Cell* **23**, 2302-2313.
- Singh, M. K., Ren, F., Giesemann, T., Bosco, C. D., Pasternak, T. P., Blein, T., Ruperti, B., Schmidt, G., Aktories, K., Molendijk, A. J. et al. (2013). Modification of plant Rac/Rop GTPase signalling using bacterial toxin transgenes. *Plant J.* **73**, 314-324.
- Sorek, N., Gutman, O., Bar, E., Abu-Abied, M., Feng, X., Running, M. P., Lewinsohn, E., Ori, N., Sadot, E., Henis, Y. I. et al. (2011). Differential effects of prenylation and S-acylation on type I and II ROPS membrane interaction and function. *Plant Physiol.* **155**, 706-720.
- Thole, J. M., Perroud, P.-F., Quatrano, R. S. and Running, M. P. (2014). Prenylation is required for polar cell elongation, cell adhesion, and differentiation in *Physcomitrella patens*. *Plant J.* **78**, 441-451.
- van Gisbergen, P. A. C., Li, M., Wu, S.-Z. and Bezanilla, M. (2012). Class II formin targeting to the cell cortex by binding PI(3,5)P(2) is essential for polarized growth. *J. Cell Biol.* **198**, 235-250.
- Veitia, R. A. and Birchler, J. A. (2010). Dominance and gene dosage balance in health and disease: why levels matter! *J. Pathol.* **220**, 174-185.
- Venus, Y. and Oelmüller, R. (2013). Arabidopsis ROP1 and ROP6 influence germination time, root morphology, the formation of F-Actin bundles, and symbiotic fungal interactions. *Mol. Plant* **6**, 872-886.
- Vidali, L., Augustine, R. C., Kleinman, K. P. and Bezanilla, M. (2007). Profilin is essential for tip growth in the moss *Physcomitrella patens*. *Plant Cell* **19**, 3705-3722.
- Vidali, L., Rounds, C. M., Hepler, P. K. and Bezanilla, M. (2009a). Lifeact-mEGFP reveals a dynamic apical F-actin network in tip growing plant cells. *PLoS ONE* **4**, e5744.
- Vidali, L., van Gisbergen, P. A. C., Guérin, C., Franco, P., Li, M., Burkart, G. M., Augustine, R. C., Blanchoin, L. and Bezanilla, M. (2009b). Rapid formin-

mediated actin-filament elongation is essential for polarized plant cell growth. *Proc. Natl. Acad. Sci. USA* **106**, 13341-13346.

Vidali, L., Burkart, G. M., Augustine, R. C., Kerdavid, E., Tüzel, E. and Bezanilla, M. (2010). Myosin XI Is essential for tip growth in *Physcomitrella patens*. *Plant Cell* **22**, 1868-1882.

Winge, P., Brembu, T., Kristensen, R. and Bones, A. M. (2000). Genetic structure and evolution of RAC-GTPases in *Arabidopsis thaliana*. *Genetics* **156**, 1959-1971.

Xu, T., Wen, M., Nagawa, S., Fu, Y., Chen, J.-G., Wu, M.-J., Perrot-Rechenmann, C., Friml, J., Jones, A. M. and Yang, Z. (2010). Cell surface- and Rho GTPase-based auxin signaling controls cellular interdigitation in *Arabidopsis*. *Cell* **143**, 99-110.

Zhang, C., Kotchoni, S. O., Samuels, A. L. and Szymanski, D. B. (2010). SPIKE1 signals originate from and assemble specialized domains of the endoplasmic reticulum. *Curr. Biol.* **20**, 2144-2149.